Engineering Computations Vol. 25 No. 6, 2008, pp. 569-588

A coupled numerical approach for nonlinear dynamic fluid-structure interaction analysis of a near-bed submarine pipeline

Y. T. Gu and Q. Wang

School of Engineering Systems
Queensland University of Technology
GPO Box 2434, Brisbane, QLD 4001 Australia
E-mail: yuantong.gu@qut.edu.au

Authors' details:

1) Y. T. GU

Lecturer
Queensland University of Technology, Australia

Mailing address:

School of Engineering System,
Queensland University of Technology,
GPO Box 2434, Brisbane, QLD 4001,Australia
Tel.:+61-7-31381009
Fax: +61-7-31381469
E-mail: yuantong.gu@qut.edu.au

2) Q. Wang

Postdoctoral Research Fellow

Proposed short title: **An approach for fluid-structure interaction analysis of a submarine pipeline**

Engineering Computations Vol. 25 No. 6, 2008, pp. 569-588

A coupled numerical approach for nonlinear dynamic fluid-structure interaction analysis of a near-bed submarine pipeline

Abstract

The near-bed submarine pipeline is a widely used structure in the marine engineering. Due to the presence of the seabed resulting in an asymmetric flow, a large negative lift (attraction) can be induced on a pipeline in a horizontal current, which has significant influence on the behaviours of the pipeline. A coupled numerical approach is proposed in this paper to assess the nonlinear dynamic responses of this pipeline by combining the meshless technique and the boundary element method (BEM). BEM is firstly used to get the nonlinear dynamic fluid loading induced by the asymmetric flow. The meshless technique is used to discretize the structure of the pipeline, and the local weighted weak form using the spline weight function is employed to get the discrete system of equations for this nonlinear dynamic analysis. A numerical example for the static and dynamic analyses of a structure is firstly presented to verify the effectivity of the present method. Then, the coupled technique is used to simulate the nonlinear dynamic fluid-structure interaction problem of a near-bed pipeline. A Newton-Raphson iteration procedure is used herein to solve the nonlinear system of equations, and the Newmark method is adopted for the time integration. Our studies reveal that there exists a critical current velocity, above which the pipeline will become instable sharply. The detailed relationship between the critical velocity and the gap is given, and it has been found that the critical velocity is significantly affected by the initial gap from the pipeline to seabed. It has demonstrated that present approach is very effective to obtain numerical solutions for the nonlinear dynamic fluid-structure interaction analysis of a near-bed submarine pipeline.

Keywords: Fluid-structure interaction, Submarine pipeline, Numerical modelling, Coupled technique, Meshless method, Nonlinear dynamic analysis

Engineering Computations Vol. 25 No. 6, 2008, pp. 569-588

1. Introduction

The near-bed submarine pipeline is a widely used structure in the marine engineering, for example the submarine gas and oil pipes. Several environmental forces have significant influences on the behaviors of these near-bed submarine pipelines. The common loadings for the pipeline are usually induced by waves and currents (lift, drag, scour), seafloor soils movements (mudslides, earthquake, sand wave migration), accidental loading (impact, underwater explosion), etc, As a complicated fluid-structure interaction problem, the behaviors of submarine pipelines subjected to various loadings have been extensively studied both theoretically and experimentally (Fredsøe and Hansen, 1987; Neill and Hinwood, 1998; Kershenbaum et al., 2000; Zong and Lam, 2000). In the absence of seabed, a submarine pipeline in a horizontally steady current experiences a zero net force in the vertical direction due to flow symmetry. However, the presence of seabed changes the symmetric flow scenario by assigning higher velocity to the flow between the pipeline and seabed, and lower velocity to the flow above the pipeline. When the gap between the pipeline and seabed is very narrow, a very high flow velocity is expected from continuity equation of fluid. From the well-known Bernoulli's equation, the pressure in the gap between the pipeline and seabed is very low, and the pressure of the flow above the pipeline is high, resulting in a downward (negative life) force (Kalghatgi & Sayer, 1997; Lam et al., 2002), which tends to pull the submarine pipeline down to seabed, exerting high bending stresses in the pipeline.

Lam et al. (2002) developed a semi-analytical method to study the static properties of the near-bed pipe by simplifying the pipe as a fixed-fixed Bernulli-Euler beam (neglecting the shear deformation) subjected to a static nonlinear fluid force. For many practical applications, the current changes with time, hence the nonlinear fluid loading becomes time-dependent and this fluid-structure interaction problem will change to a nonlinear dynamic problem, which will be studied in this paper. In addition, the semi-analytical technique will be not suitable for many practical pipes, especially for problems with complex boundary conditions and with significant transverse shear deformation. An effective numerical modelling and simulation technique is necessary for this nonlinear dynamic fluid-structure interaction analysis. To the best of our knowledge, there are very rare such studies, if any. In this paper, following the technique used by Lam et al. (2002), for a given time step, the nonlinear loading is firstly obtained by the

boundary element method (BEM). The advanced local meshless method is used to discretize the pipe structure (the thick beam). We focus on the analysis of the global response of the pipe, therefore, it is reasonable that the pipe is simplified as a thick beam, in which the transverse shear deformation is considered.

In recent years, more and more researchers are devoting themselves to the research of the meshless methods, due to the fact that there are still many spaces in the development of meshless methods. Detailed reviews of meshless methods can be found in the monograph (Liu and Gu, 2005). There are many categories of meshless methods, and group of meshless methods have been developed including the strong meshless methods(Mai-Duy, 2006), the smooth particle hydrodynamics (SPH) (Gingold and Monaghan, 1977), the element-free Galerkin (EFG) method (Belytschko et al., 1994; Kanok-Nukulchai et al., 2001; Noguchi et al., 2000), the reproducing kernel particle method (RKPM) (Liu et al., 1995; Liew et al. 2002), and the point interpolation method (PIM) (Liu and Gu, 2001a; Liew and Chen, 2004). In order to alleviate the global integration background cells, the meshless methods based on the local weak-forms have also been developed, for example, the meshless local Petrov-Galerkin (MLPG) method (Atluri and Shen, 2002; Gu and Liu, 2001a), the local radial point interpolation method (LRPIM) (Gu and Liu, 2001b; Liu and Gu, 2001b; Gu et al., 2007), and weak-strong form method (Gu and Liu, 2005; Liu and Gu, 2003) .

Because the local meshless methods do not require a global background mesh for numerical integration of the global weak form, they are truly meshless and have been widely used. Hence, the local meshless technique will be used in this paper. The nonlinear dynamic system of equations is obtained based on the meshless shape function and the weighted local weak form of the governing equation of a near seabed pipeline motion in current (by equating nonlinear fluid force to bending force). The well-developed Newmark method (Zienkiewicz and Taylor, 2000) and the Newton-Raphso iteration technique are used to directly solve the nonlinear dynamic system of equations.

Our investigations reveal that the negative lift is so large that it is likely for submarine pipelines to fail even in normal operational environments. There exists a critical current velocity, above which a near-seabed pipeline will become instable and finally fully rest on seabed. Below the critical velocity, a near-seabed pipeline, even in stable state, may also have high bending stress. The relationship between critical velocity and gap between pipeline and

seabed is given. It has been found that the present method is very easy to implement, and very efficient to obtain numerical solutions for the nonlinear dynamic fluid-structure interaction analysis of a near-bed submarine pipeline.

2. Nonlinear dynamic fluid force for a near-bed pipeline

Fluid–structure interaction is a common phenomenon in nature and can be found in many engineering applications. In the simulation of fluid–structure interaction, we need calculate the fluid forces which act on the structure. Many methods have been developed to solve the fluid–structure interaction problems. Bathe et al. (2001, 2004) have developed a FEM model of fluid flows fully coupled with structural interactions. Glowinski et al. (1991) proposed a fictitious domain method for the numerical solutions of 3D elliptic problems with Dirichlet boundary conditions for modelling incompressible viscous flow. Tai and Liew et al. (2007) developed an immersed object method for 3D unsteady flow simulation with fluid–structure interaction. In this paper, we will use BEM coupled with the rational approximation (Lam et al., 2002) to obtain the dynamic fluid force for a near-bed pipeline.

Consider a circular steel pipe covered with a layer of reinforced concrete. The coordinate system is shown in Figure 1. The current velocity is $U(t)$, where t is time, and the gap (distance) between the central line of the undeformed pipeline and seabed is D_0. The fluid is assumed irrotational and incompressible, so there is a potential $\phi(x,y,z)$ due to the presence of the pipeline, satisfying (Lam et al., 2002):

$$\frac{\partial^2\phi}{\partial x^2}+\frac{\partial^2\phi}{\partial y^2}+\frac{\partial^2\phi}{\partial z^2}=0, \qquad \text{Throughout the fluid domain} \tag{1}$$

$$\frac{\partial\phi}{\partial y}=U(t), \qquad \sqrt{x^2+y^2+z^2}\to\infty \tag{2}$$

$$\frac{\partial\phi}{\partial n}=0, \qquad \text{On the pipe surface} \tag{3}$$

where $n=(n_x,n_y,n_z)$ denotes the three-dimensional unit vector normal to the pipe surface.

A lot of computation efforts are needed to solve the equations above due to the nature of three-dimensional flow. However, the computation can be greatly simplified by using slenderness assumption (Newman 1978) defined by the following relations,

$$\varepsilon=R_c/L<<1, \quad n_x=O(\varepsilon),\ n_y=O(1),\ n_z=O(1) \tag{4}$$

On this basis, near the surface of the pipe, we have

$$\frac{\partial \phi}{\partial x} << \left(\frac{\partial \phi}{\partial y}, \frac{\partial \phi}{\partial z}\right), \ \frac{\partial^2 \phi}{\partial x^2} << \left(\frac{\partial^2 \phi}{\partial y^2}, \frac{\partial^2 \phi}{\partial z^2}\right) \tag{5}$$

Thus Laplace's equation reduces to a two-dimensional format (Lam et al. 2002) using $\boldsymbol{\Phi}$ to replace the three-dimensional potential

$$\frac{\partial^2 \boldsymbol{\Phi}}{\partial y^2} + \frac{\partial^2 \boldsymbol{\Phi}}{\partial z^2} = 0, \quad \boldsymbol{\Phi} = \phi(y, z; x) \tag{6}$$

Here the dependence on x is included to emphasize that this potential will vary slowly along the structure length, as a result of the change in the lateral deformation. The boundary conditions (2) and (3) can then be replaced by

$$\frac{\partial \boldsymbol{\Phi}}{\partial y} = U(t), \qquad \sqrt{y^2 + z^2} \to \infty \tag{7}$$

$$\frac{\partial \boldsymbol{\Phi}}{\partial N} = 0, \qquad \text{On the pipe surface} \tag{8}$$

Here $N = (N_y, N_z)$ denotes the two-dimensional unit vector normal to the pipe surface in the $y - z$ plane. The potential $\boldsymbol{\Phi}$ corresponds to the solution of a two-dimensional flow problem at each section along the pipe length, and thus is easily found.

Based on 2-D assumption, the boundary-value problem defined by Equations (5)~(8) can be effectively solved using the traditional boundary element method (BEM) (Brebbia, 1978). The semi-infinite fluid domain is approximated by a rectangular domain Ω (i.e., $20R_c \times 20R_c$), and it is discretized by m constant BE elements. BEM solution to Equations (5)~(8) is

$$\frac{1}{2}\boldsymbol{\Phi}^i + \sum_{j=1}^{m} \boldsymbol{\Phi}_j \int_{\Gamma_j} \frac{\partial \boldsymbol{\Phi}^*}{\partial N} d\Gamma = \sum_{j=1}^{m} \frac{\partial \boldsymbol{\Phi}}{\partial N} \int_{\Gamma_j} \boldsymbol{\Phi}^* d\Gamma \tag{9}$$

where $\boldsymbol{\Phi}^i$ is the potential for a point i on the boundary, and $\boldsymbol{\Phi}^* = \frac{1}{2\pi} \ln \frac{1}{r}$, is the fundamental solution. Equation (9) can be written in matrix form (Brebbia, 1978),

$$\mathrm{H}\ \Phi = \mathrm{Q} \tag{10}$$

where

$$H_{ij} = \int_{\Gamma_j} \frac{\partial \boldsymbol{\Phi}^*}{\partial N} d\Gamma + \frac{\delta_{ij}}{2} \tag{11}$$

$$Q_i = \sum_{j=1}^{m} \frac{\partial \boldsymbol{\Phi}_j}{\partial N} \int_{\Gamma_j} \boldsymbol{\Phi}^* d\Gamma \tag{12}$$

Solving Equation (10) with boundary conditions, the distributed potential **Φ** can be obtained. Tangential and normal velocities on the pipe surface are given, respectively

$$v_t = \frac{\partial \Phi}{\partial t}, \qquad v_n = 0 \tag{13}$$

where *n* and *t* are the unit outward normal and tangent, respectively, to the pipe surface. From Bernoulli's equation, the flow pressure *p* on the pipe surface can be obtained

$$p = -\frac{1}{2}\rho(v_t + v_n)^2 \tag{14}$$

where ρ is water density.

Integrating *p* along the section, we obtain the downward fluid force *f* on the pipe, as shown in Figure 2:

$$f = \oint_C p\ n_z dl \tag{15}$$

where n_z is the unit vertical vector. Substituting Equation (14) into Equation (15), we can compute the fluid force and BEM results have been plotted in Figure 3.

Although there exists an analytical solution for this fluid force (Müller, 1929), the complex formulation converges very slowly. Therefore, for the computational efficiency, Lam et al. (2002) used a rational approximation (the least-square fitting) to fit the fluid force obtained by BEM. The following result was obtained from Figure 3 (Lam et al., 2002) and will be used in this paper

$$c(d) = \frac{2.23d^2 + 12.54d + 0.02}{0.77d^3 + 0.44d^2 + 0.02d} \tag{16}$$

where the dimensionless coefficients are defined

$$c = \frac{2f}{\rho A U(t)^2} \tag{17}$$

$$d = \frac{D_0 - w(x,t) - R_s}{2R_s} \tag{18}$$

where *A* is the cross section area.

The BEM result, the least-square (LS) fitting result and the analytical result are shown in Figure 3. We can find from this figure that these results are in very good agreement. It has validated that the approach used in this paper to obtain the fluid force is very accurate. Using

this fitting curve, the nonlinear fluid forces for every iteration step can be easily obtained. Hence, the fluid force induced by the current can be explicitly written as

$$f(t) = \frac{1}{2}\rho A U(t)^2 c(d) \tag{19}$$

The force f is a nonlinear function of the deflection.

It should be mentioned here that the two-dimensional inviscid simplification is used, the fluid force is infinite when the gap $D_0 \to 0$. If a three-dimensional model is used for the fluid domain, the force will be finite when $D_0 \to 0$ (Zong and Lam, 2000).

3. Local meshless formulation for the nonlinear dynamic analysis

In this paper, we focus on the global dynamic response of a near-bed pipeline. It has been justified by Lam et al. (2002) that using the beam simplification can obtain satisfactory results for this problem. For many practical applications, the shear deformation cannot be neglected, so the pipe can be simplified as a thick beam fixed at both ends. The non-damping governing motion equation of a this pipeline can be written as (Reddy, 1993)

$$\begin{cases} \rho A \dfrac{\partial^2 w}{\partial t^2} - \dfrac{\partial}{\partial x}[GAk_s(\dfrac{\partial w}{\partial x} + \theta)] - f = 0 \\ \rho I \dfrac{\partial^2 \theta}{\partial t^2} - \dfrac{\partial}{\partial x}(EI\dfrac{\partial \theta}{\partial x}) + GAk_s(\dfrac{\partial w}{\partial x} + \theta) = 0 \end{cases} \tag{20}$$

where w is the deflection of the beam, θ is the rotation, ρ is the mass density, E is the modulus of elasticity, I is the moment of inertia, A is the cross section area, G is the shear modulus, and k_s is the shear correction coefficient. From Figure 1, we can obtain

$$A = \pi[R_s^2 - (R_s - t_s)^2] \tag{21}$$

$$I = \frac{1}{4}\pi[R_s^4 - (R_s - t_s)^4] \tag{22}$$

The auxiliary boundary and initial conditions are given as

$$w(x_0) = \overline{w}, \quad \text{on } \Gamma_w, \tag{23}$$

$$\theta(x_0) = \overline{\theta}, \quad \text{on } \Gamma_\theta$$

$$M(x_0) = EI\frac{\partial \theta}{\partial x}\bigg|_{x=x_0} = \overline{M}, \quad \text{on } \Gamma_M; \tag{24}$$

$$V(x_0) = GAk_s(\theta + \frac{\partial w}{\partial x})\Big|_{x=x_0} = \overline{V}, \quad \text{on } \Gamma_V$$

$$w(x,t_0) = w_0(x), \quad \text{in } \Omega, ; \qquad \theta(x,t_0) = \theta_0(x), \quad \text{in } \Omega \tag{25}$$

$$\frac{\partial w(x,t_0)}{\partial t} = v_0(x) \quad \text{in } \Omega ; \qquad \frac{\partial \theta(x,t_0)}{\partial t} = \gamma_x(x), \quad \text{in } \Omega \tag{26}$$

where Γ_w, Γ_θ, Γ_M, and Γ_V are the boundaries of w, θ, M, and V satisfying, respectively. t is the time, and the t_0 is the initial time. It should be mentioned here that for the fixed-fixed beam $\overline{w} = \overline{\theta} = 0$.

The local weak form of the partial differential equation (20), over a local support domain Ω_s bounded by Γ_s, can be obtained using the local weighted residual method

$$\begin{aligned} &\int_{\Omega_s} \hat{w}\{\rho A\frac{\partial^2 w}{\partial t^2} - \frac{\partial}{\partial x}[GAk_s(\frac{\partial w}{\partial x} + \theta)] - f\}d\Omega = 0 \\ &\int_{\Omega_s} \hat{w}[\rho I\frac{\partial^2 \theta}{\partial t^2} - \frac{\partial}{\partial x}(EI\frac{\partial \theta}{\partial x}) + GAk_s(\frac{\partial w}{\partial x} + \theta)]d\Omega = 0 \end{aligned} \tag{27}$$

where $\hat{w}$ is the weight function.

It can be found that the boundary Γ_s for the local support domain is usually composed by five parts (Gu and Liu, 2001b): the internal boundary Γ_{si}, the boundaries Γ_{sw}, $\Gamma_{s\theta}$, Γ_{sM}, and Γ_{sV}, over which the essential boundary conditions w, θ and natural boundary conditions M, V are specified. The boundaries Γ_{sw} with Γ_{sV} and $\Gamma_{s\theta}$ with Γ_{sM} are mutually disjoint. Integrating Equation (18) by parts and imposing the natural boundary condition, we obtain

$$\begin{aligned} &\int_{\Omega_s} \hat{w}\rho A\frac{\partial^2 w}{\partial t^2}d\Omega + \int_{\Omega_s}[\frac{\partial \hat{w}}{\partial x}GAk_s(\frac{\partial w}{\partial x} + \theta) - \hat{w}f]d\Omega \\ &\qquad -[\overline{n}\hat{w}\overline{V}]\Big|_{\Gamma_{sV}} - [\overline{n}\hat{w}GAk_s(\frac{\partial w}{\partial x} + \theta)]\Big|_{\Gamma_s - \Gamma_{sV}} = 0 \\ &\int_{\Omega_s} \hat{w}\rho I\frac{\partial^2 \theta}{\partial t^2}d\Omega + \int_{\Omega_s}[\frac{\partial \hat{w}}{\partial x}(EI\frac{\partial \theta}{\partial x}) + \hat{w}GAk_s(\frac{\partial w}{\partial x} + \theta)]d\Omega \\ &\qquad -[\overline{n}\hat{w}\overline{M}]\Big|_{\Gamma_{sM}} - [\overline{n}\hat{w}(EI\frac{\partial \theta}{\partial x})]\Big|_{\Gamma_s - \Gamma_{sM}} = 0 \end{aligned} \tag{28}$$

Considering the deflection, w, and the rotation, θ, as independent variables, and only the space domain to be discretized, we can have

$$w(x,t) = \mathbf{\Phi}_w(x)\mathbf{w}_e(t), \qquad (29)$$

$$\theta(x,t) = \mathbf{\Phi}_\theta(x)\boldsymbol{\theta}_e(t)$$

where $\mathbf{\Phi}_w(x)$ and $\mathbf{\Phi}_\theta(x)$ are meshless shape functions of the deflection and the rotation, respectively. They can be constructed using polynomial point interpolation (Liu and Gu, 2005). $\mathbf{w}_e(t)$ and $\boldsymbol{\theta}_e(t)$ are nodal values of deflections and rotations. The discretized system equation can be obtained as

$$\mathbf{M}\ddot{\mathbf{u}}(t) + \mathbf{K}\mathbf{u}(t) = \mathbf{f}(\mathbf{u},t) \qquad (30)$$

where $\mathbf{M}$ and $\mathbf{K}$ are the mass matrix and the stiffness matrix, respectively. $\mathbf{u}(t)$ is the vector of nodal deflections and rotations, $\ddot{\mathbf{u}}(t)$ is the second order derivative of $\mathbf{u}(t)$ related to time t, and $\mathbf{f}$ is the vector of the external force. Hence,

$$\mathbf{u}(t) = \{w_1, \theta_1, \cdots, w_n, \theta_n\}^{\mathrm{T}} \qquad (31)$$

Elements of $\mathbf{M}$, $\mathbf{K}$ and $\mathbf{f}$ can be written as

$$m_{ij}^{11} = \int_{\Omega_s} \rho A \widehat{w}_i \Phi_j^w d\Omega, \quad m_{ij}^{12} = m_{ij}^{21} = 0, \quad m_{ij}^{22} = \int_{\Omega_s} \rho I \widehat{w}_i \Phi_j^\theta d\Omega \qquad (32)$$

$$k_{ij}^{11} = \int_{\Omega_s} GAk_s \frac{d\widehat{w}_i}{dx}\frac{d\Phi_j^w}{dx} d\Omega + [\bar{n}GAk_s \widehat{w}_i \frac{d\Phi_j^w}{dx}]\Big|_{\Gamma_{si}+\Gamma_{sw}+\Gamma_{s\theta}+\Gamma_{sM}}, \qquad (33)$$

$$k_{ij}^{12} = \int_{\Omega_s} GAk_s \frac{d\widehat{w}_i}{dx}\Phi_j^\theta d\Omega + [\bar{n}GAk_s \widehat{w}_i \Phi_j^\theta]\Big|_{\Gamma_{si}+\Gamma_{sw}+\Gamma_{s\theta}+\Gamma_{sM}},$$

$$k_{ij}^{21} = \int_{\Omega_s} GAk_s \widehat{w}_i \frac{d\Phi_j^w}{dx} d\Omega,$$

$$k_{ij}^{22} = \int_{\Omega_s} (EI\frac{d\widehat{w}_i}{dx}\frac{d\Phi_j^\theta}{dx} + GAk_s \widehat{w}_i \Phi_j^\theta) d\Omega + [\bar{n}EI\widehat{w}_i \frac{d\Phi_j^\theta}{dx}]\Big|_{\Gamma_{si}+\Gamma_{sw}+\Gamma_{s\theta}+\Gamma_{sV}}$$

$$f_i^w = \int_{\Omega_s} \widehat{w}_i f(\mathbf{u},t) d\Omega + [\bar{n}\widehat{w}_i \bar{V}]\Big|_{\Gamma_{sV}}, \qquad f_i^\theta = [\bar{n}\widehat{w}_i \bar{M}]\Big|_{\Gamma_{sM}} \qquad (34)$$

The dynamic Equation (30) can be solved by several direct analysis methods. Among them, the Newmark method is an unconditionally stable method when its coefficients satisfy $\delta \geq 0.5$ and

$\beta \geq \frac{1}{4}(\delta + 0.5)^2$ (Zienkiewicz and Taylor, 2000). It will be used in the following numerical studies for the time integration. In each time step, the nonlinear equation has to be solved because of the nonlinear loading. A Newton-Raphson iteration method is used to solve the nonlinear dynamic system of equations. The iteration will stop when the following criteria is satisfied.

$$\sqrt{\sum_{j=1}^{n}(w_j^{i+1} - w_j^i)^2} \leq \varepsilon \tag{35}$$

where n is the number of nodes used, w_j^i and w_j^{i+1} are the deflection results of the ith and $(i+1)$th iteration steps, respectively. ε is a specified accuracy tolerance.

It should be mentioned here that in the numerical simulation for beam problems, there is shear-locking phenomenon using the thick beam model when the length and thickness ratio of a beam becomes much larger. Some researches have reported (Liu 2002) that the meshfree technique based on the meshless shape functions can overcome the shear-locking problem if the order of the interpolation is sufficient high. In the following numerical studies, more than 5 field nodes are used in meshfree interpolation (the shape function with high order), hence, the shear-locking issue will be overcome automatically. Of course, the numerical integration should be also accurate enough(in this paper, 4 Gaussian points are used for each background cell).

4. Numerical results

4.1. Verification of a cantilever beam

To verify the present method, a cantilever thick beam, as shown in Figure 4, is analyzed. The parameters of this beam are: E=3.0×10^7 N/m^2, $\bar{v}$ =0.3, L=48m, D=12m, $\bar{t}$ =1.0m, and the concentrated force $f(L)$=1000 $g(t)N$, where $g(t)$ is the function of time. In this example, L/D=4, hence it should be considered as a thick beam. The analytical solution for static analysis is available in the text book (Timoshenko and Goodier, 1970)

$$w(x) = -\frac{f(L)}{6EI}\left[(4+5\bar{v})\frac{D^2x}{4} + (3L-x)x^2\right] \tag{36}$$

Deflections obtained by the present method are plotted in Figure 5. The negative values show the deflections are downward. It can be found that the results obtained by the present method agree with the analytical solution, with the discrepancy less than 0.6%.

In the numerical convergence study, several groups of regularly and evenly distributed field nodes are used. The convergence curve obtained numerically is shown in Figure 6, where *h* is equivalent to the nodal space (in *x* direction). The error is defined as (Liu 2002)

$$error = \frac{\sqrt{\int_\Omega (w_{num} - w_{exact})^2 d\Omega}}{\sqrt{\int_\Omega w_{exact}{}^2 d\Omega}} \tag{37}$$

where w_{num} and w_{exact} are deflections of the beam obtained by numerical methods and the analytical method, respectively. The integration is performed over the entire span of the beam. From Figure 6, we can find that the present method has good convergent. The convergence rate that is computed via linear regression can also be obtained from Figure 6, and the convergence rate of the present method is about 1.5. Hence, it has proven that the present technique has very good convergence.

For dynamic analysis, we consider $g(t) = \sin(\omega_f t)$, where ω_f is the frequency of the dynamic load, and ω_f=27 is used in this example. Many time steps are calculated to check the stability of the presented method. The Newmark method with $\Delta t = 5\times10^{-3}$ is used for the time integration, and the damping coefficient, *c*=0.4, is considered. Results until to 20s (about 100 natural vibration periods) are plotted in Figure 7, which shows a very stable result obtained by the present method. After a long period time, the forced vibration under a simple harmonic dynamic loading becomes a stable vibration with the forced frequency ω_f. Compared with the results obtained by Gu and Liu (2001a), the present method leads to a very agreement result.

From the vibration theory (Meirovitch, 1980), a resonance will occur when $\omega_f = \omega_i$, where ω_i is the *i*-th natural frequency. From Figure 7, one can observe that the amplitude of vibration is very big (i.e. more than ten times of static displacement) because ω_f is very close to ω_1. In addition, a beat vibration with the period T_b occurs when $\omega_f \approx \omega_1$ and $T_b = \dfrac{2\pi}{|\omega_f - \omega_1|}$. The first

natural frequency of the system has been obtained by FEM (Gu and Liu, 2001a), which is $\omega_1^{FEM} = 28.2$, and, hence, $T_b^{FEM} \approx 5.2$. T_b can be also obtained from Figure 7, and it is around 4.5. It has also proven that the present method obtained very good results for this dynamic analysis of this thick beam problem.

4.2. Nonlinear dynamic analysis of a near-bed pipeline

Consider the following pipeline, as shown in Figure 1: L = 20 *m*, E_s =2.11× 10^{11} *N/m*^{2}, R_s =0.4 *m*, t_s= 0.012 *m* (steel pipe thickness), E_c=2.5× 10^{10} *N/m*^{2}, R_c=0.5 *m*, ρ_s=7800 *kg/m*^{3} (steel density), ρ_c=2400 *kg/m*^{3} (concrete density), D_0=2R_c. The pipe is discretized by 40 regularly distributed meshless nodes.

Firstly, the nonlinear static response for a constant current is analyzed. Figure 8 gives the relation between current velocity U and mid-span deflection $W_{L/2}$. The values of mid-span deflection change with the current velocities. In the simulation of the near-bed pipeline, we find a sharp instability in the behavior of the pipeline. As the current velocity increases, the deflection of the pipeline increases, and the gap between the pipe and the seabed decreases. It can be found that when the current velocity increases to one certain value, the pipe becomes instable and the centre of the pipe (because two ends are fixed) will touch the bed (i.e., the gap is 0). This process is defined as the *critical pull-in behavior* and the "certain value" of the current velocity is defined as the *critical pull-in velocity*, U^{cr}. From Figure 8, we can obtain that the critical pull-in velocity for this pipeline is $U^{cr} = 9.10\, m/s$. Compared with the value obtained through the semi-analytical method (Lam et al., 2002), which is 9.29m/s, the present coupled method obtains good result, and it has validate the new developed model in this paper.

It is clear from the above discussion that the critical velocity U^{cr} is dependent on the initial gap between the pipeline and seabed. Such relation is obtained by repeatedly using Equation (30) for different D_0, and is plotted in Figure 9. Physically, a small gap between pipeline and seabed will induce a high force on the pipeline as seen from Equation (19) or Figure 3. The required current velocity to push pipeline to seabed is then low. The relationship is shown in Figure 9, in which U_{cr} is a monotonically increasing function of D_0. The results obtained by the model (Lam et al., 2002) without considering the transverse shear deformation are also plotted in Figure 9. It can be found that critical pull-in velocity U^{cr} will be smaller with considering the

transverse shear deformation than that without considering. It is because that considering the transverse shear deformation will increase the global deflection. It should be mentioned here that the difference of U^{cr} for these two models will enlarge when $L/2R_c$ decreases.

In the nonlinear dynamic analysis, we consider the current velocity $U(t) = U_0 \cdot k(t)$ is time-dependent. Two cases are considered for $k(t)$, as shown in Figure 10. To reveal the influence of the shear deformation, a shorter pipeline with L=10m is analyzed (for this pipeline the semi-analytical method is inapplicable because it cannot be simplified as a Bernulli-Euler beam). The deflections at the central point ($x=L/2$) of the pipe are obtained and plotted in Figures11-16.

U_0=5m/s and $k_1(t)$ is firstly studied. Figure 11 shows the beginning stage of the nonlinear dynamic response. The vibration frequency can be easily obtained from this figure. The dynamic responses of $U(t)$=5$\cdot$ $k_1(t)$ m/s and 10$\cdot$ $k_1(t)$ m/s for a longer computational time are plotted in Figures 12 and 13, respectively. It can be found that the response below the undeformed position is a stable vibration because of the unchanged current velocity during 0~0.5s. As the current velocity declines during 0.5~0.7s, the deflection of the pipe becomes smaller. After 0.7s, the current velocity becomes zero, and the dynamic response of the pipe becomes stable vibration again, in which the equilibrium position is x-axis (the undeformed pipe). This stable vibration is obtained under the neglect of the damping. If the damping is considered, the response will be declined with time until the vibration vanishes. The similar tendency can be found for the case of $k_2(t)$, as shown in Figures 14 and 15. From Figures 12-15, it can be observed that the present method can lead to very stable results for this nonlinear dynamic analysis.

There is also critical pull-in behavior for this pipeline under the time-depend current. For the case of $k_1(t)$, the dynamic critical pull-in velocity U_0^{crit} is around 16 m/s, which is smaller than that of the same pipeline under the static current, which is lager than 18 m/s.

Figure 16 demonstrates the relationship between the maximum deflection of the central point ($x=L/2$) of the pipe and U_0. The time function $k_1(t)$ is used here to investigate the change of the deflections for given U_0. From this figure, we can find that the maximum deflection monotonously increases as U_0 increases. For the same U_0, the maximum deflections during 0~0.5s are greater than those after 0.7s. This is because the current velocity becomes zero after

0.7s, there will be no fluid force on the pipe. In evidence, the pipe will be risk if the velocity U_0 is large.

5. Conclusion and discussion

In this paper, the nonlinear dynamic fluid-structure interaction of a near-bed pipeline is analyzed by a coupled numerical approach based on the meshless technique and BEM. BEM is firstly used to get the nonlinear dynamic fluid loading induced by the asymmetric flow. The local meshless technique is then used to discretize the structure of the pipeline. The Newmark method and Newton-Raphson iteration technique are adopted to solve the nonlinear dynamic system of equations. Numerical examples are presented and the results have been compared with the results obtained by the analytical and semi-analytical methods. From the above studies, we can obtain the following conclusions:

1) Our investigations reveal that the presence of seabed will lead to a large negative lift loading on the pipeline. It will be a complex nonlinear fluid-structure interaction problem, for which the traditional numerical technique becomes very difficult to be used.
2) There exists a critical current velocity, above which a near-seabed pipeline will become instable and finally fully rest on seabed. The critical velocity changes with the initial gap between the pipeline and the seabed.
3) It is found that the present method is very easy to implement, and very effective to obtain numerical solutions for the nonlinear dynamic fluid-structure interaction analysis of a near-bed submarine pipeline.

It should be mentioned here that the major objective of this paper is to develop a new numerical approach for a special fluid-structure interaction analysis of a near-bed submarine pipeline. The fluid is assumed irrotational and incompressible, therefore, it is the ideal fluid. In the practical situation, the effects of viscous and inertia forces cannot be ignored. In addition, the 3D problems should be also considered. These will be studied in our future research work.

Acknowledgement

This work is supported by an ARC Discovery Grant.

REFERENCES

Atluri S.N. and Shen S.P. (2002), *The Meshless Local Petrov-Galerkin (MLPG) method*, Tech Sciemce Press. Encino USA.

Bathe K.J. and Zhang H. (2004), "Finite element developments for general fluid flows with structural interactions", *Int J Numer Methods Eng*., 60,213–32.

Belytschko T., Lu Y. Y. and Gu L. (1994), "Element-free Galerkin methods", *International Journal for Numerical Methods in Engineering*, 37, 229-256.

Brebbia C. A. (1978), *The boundary Element Method for engineers*, Pentench Press, London, Hastead Press, New York.

Fredsøe J. and Hansen E.A. (1987), "Lift forces on pipelines in steady flow", *Journal of Waterway, Port, Coastal and Ocean Engineering Division*, ASCE, 113, 139-155.

Gingold R.A. and Monaghan J.J. (1977), "Smooth particle hydrodynamics: theory and applications to non-spherical stars", *Monthly Notices of the Royal Astronomical Society*, 181, 375-389.

Glowinski, R., Pan, T.W. and Periaux, J.(1994), "A fictitious domain method for Dirichlet problems and applications", *Comput Methods Appl Mech Eng*. v111. 283-303.

Glowinski, R., Pan, T.W. and Periaux, J. (1994), "A fictitious domain method for external incompressible viscous flow modeled by Navier-Stokes equations", *Comput Methods Appl Mech Eng.*, 112, 133-148.

Gu Y.T. and Liu G.R. (2001a), "A meshless Local Petrov-Galerkin (MLPG) method for free and forced vibration analyses for solids", *Computational Mechanics*, 27(3), 188-198.

Gu Y. T. and Liu G. R. (2001b), "A local point interpolation method for static and dynamic analysis of thin beams", *Computer Methods in Applied Mechanics and Engineering*, 190, 5515-5528.

Gu Y.T. and Liu G.R. (2005), "A Meshfree Weak-Strong (MWS) form method for time dependent problems", *Computational Mechanics*, 35, 134 –145.

Gu Y.T., Wang Q.X. and Lam K. Y. (2007), "A Meshless Local Kriging Method for large deformation Analyses", *Computer Methods in Applied Mechanics and Engineering*, 196, 1673–1684.

Kalghatgi S.G. and Sayer P.G. (1997), "Hydrodynamics forces on piggyback pipeline configurations", *Journal of Waterway, Port, Coastal and Ocean Engineering Division*, 123, 16-22.

Kanok-Nukulchai W., Barry W.J. and Saran-Yasoontorn K. (2001), "Meshless formulation for shear-locking free bending elements", *Structural engineering and Mechanics*, 11, 123-132.

Kershenbaum N.Y., Mebarkia S.A. and Choi H.S. (2000), "Behavior of marine pipelines under seismic faults", *Ocean Engineering*, 27, 473-487.

Lam K.Y., Wang Q.X. and Zong Z. (2002), "A nonlinear fluid-structure interaction analysis of a near-bed submarine pipeline in a current", *Journal of Fluids and Structures*,16(8), 1177-1191.

Liew K.M. and Chen X.L.(2004), "Mesh-free radial point interpolation method for the buckling analysis of Mindlin plates subjected to in-plane point loads", *International Journal for Numerical Methods in Engineering*, 60(11): 1861-1877.

Liew K.M., Wu H.Y., Zou G.P. and Ng T.Y. (2002), "Elasto-plasticity revisited: numerical analysis via reproducing kernel particle method and parametric quadratic programming", *International Journal for Numerical Methods in Engineering*, 55 6 (2002), 669–683.

Liu G.R. and Gu Y.T., (2001a), "A point interpolation method for two-dimensional solid", *International Journal for Numerical Methods in Engineering*, 50, 937-951.

Liu G. R. and Gu Y. T. (2001b), "A local radial point interpolation method (LR-PIM) for free vibration analyses of 2-D solids", *Journal of Sound and Vibration*, 246 (1), 29-46.

Liu G.R. and Gu Y.T. (2003), "A meshfree method: Meshfree Weak-Strong (MWS) form method, for 2-D solids", *Computational Mechanics*, 33(1), 2-14.

Liu G.R. and Gu Y.T. (2005), An introduction to meshfree methods and their programming. Springer Press, Berlin.

Liu G.R. (2002), *Mesh Free Methods: Moving Beyond the Finite Element Method*, CRC Press LLC.

Liu W.K., Jun S., Zhang Y. (1995), "Reproducing kernel particle methods", *International Journal for Numerical Methods in Engineering*, 20: 1081-1106.

Mai-Duy N. (2006), "An effective spectral collocation method for the direct solution of high-order ODEs", *Communications in Numerical Methods in Engineering*, 22(6), 627-42

Meirovitch L (1980), "Computational Methods in Structural Dynamics", Sijthoff & Noordhoff: Grningen.

Müller W.V. (1929), **"**Systeme von Doppelquellen in der dbenen Strömung**"**, *Mathematik und Mechanik* 9, Heft 3, 200-213.

Neill I.A.R. and Hinwood J.B.(1998), "Wave and wave-current loading on a bottom-mounted circular cylinder", *International Journal of Offshore and Polar Engineering*, 8, 122-129.

Newman J. (1978), *Marine Hydrodynamics*. The MIT Press, Cambridge, MA, 362-373.

Noguchi H., Kawashima T. and Miyamura T. (2000), "Element free analysis of shell and spatial structures", *Int. J. Numer. Methods Eng.* 47, 1215–1240.

Reddy J. N.(1993), *An introduction to the Finite Element Method*. New York: McGraw Hill, 2nd edition.

Rugonyi, S. and Bathe, K.J.(2001), "On the finite element analysis of fluid flows fully coupled with structural interactions", *Comput Modeling Eng Sci.*, 2 195-212.

Tai C.H., Liew K. M. and Zhao Y.(2007), "Numerical simulation of 3D fluid-structure interaction flow using an immersed object method with overlapping grids", *Computers and Structures*, 85(11-14), 749-762.

Timoshenko S.P. and Goodier J.N. (1970), *Theory of Elasticity*, 3rd Edition. McGraw-hill, New York.

Zienkiewicz O.C. and Taylor R.L. (2000), *The finite element method* (5th ed.). Butterworth Heinemann, Oxford.

Zong Z. and Lam K.Y.(2000), "Hydrodynamics influences on the ship hull vibration in shallow water", *Journal of Engineering Mathematics*, 37, 363-374.

Engineering Computations Vol. 25 No. 6, 2008, pp. 569-588

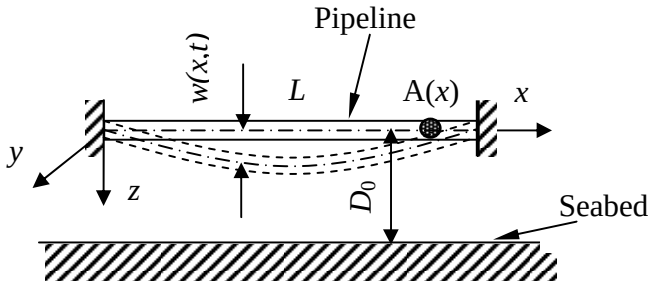

(a) The configuration of a near-bed pipeline

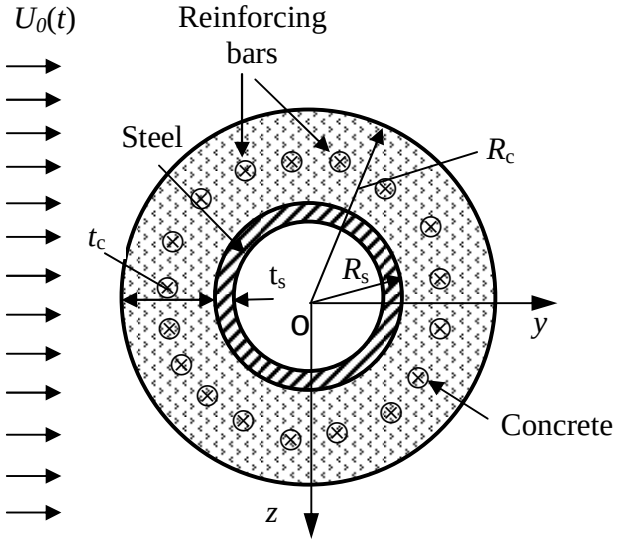

(b) The section A

Figure 1 A near-bed pipeline

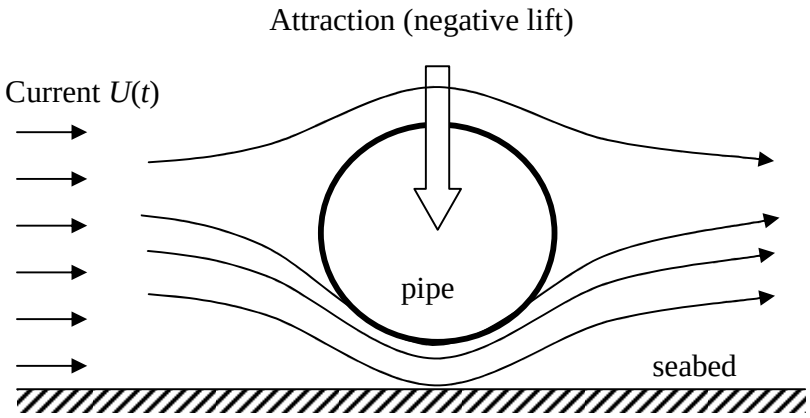

Figure 2 A near-bed submarine pipeline in the current

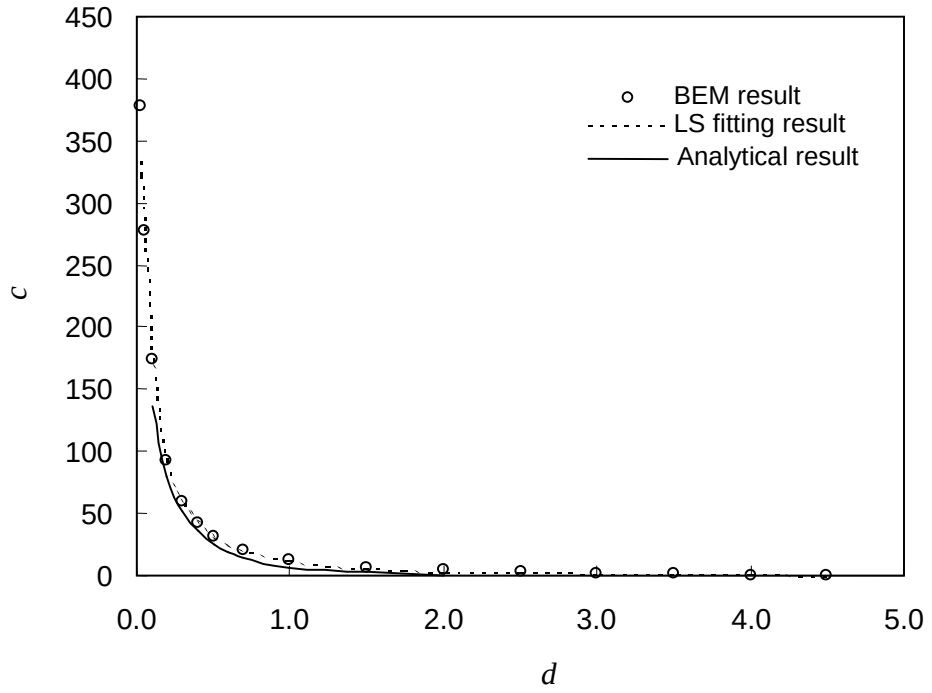

Figure 3 The dimensionless fluid force of the BEM result, the LS fitting result and the analytical result

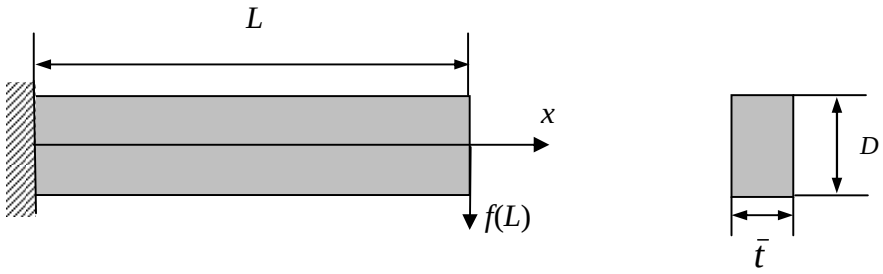

Figure 4 A cantilever thick beam

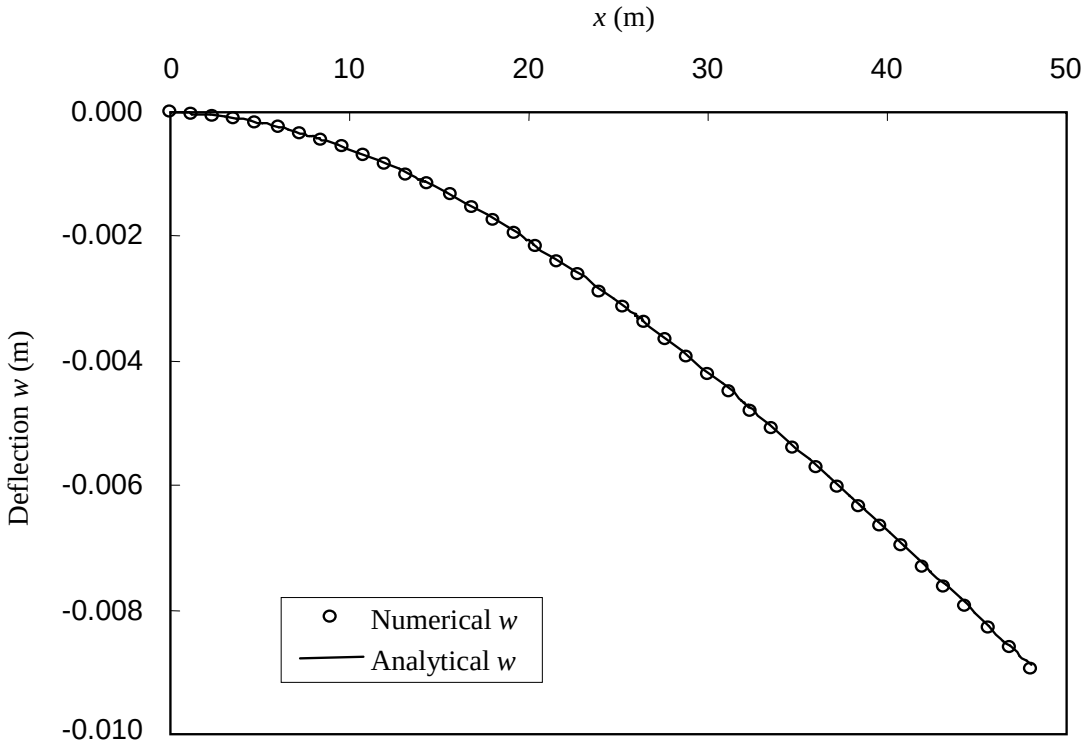

Figure 5 Static Deflection results of a cantilever thick beam

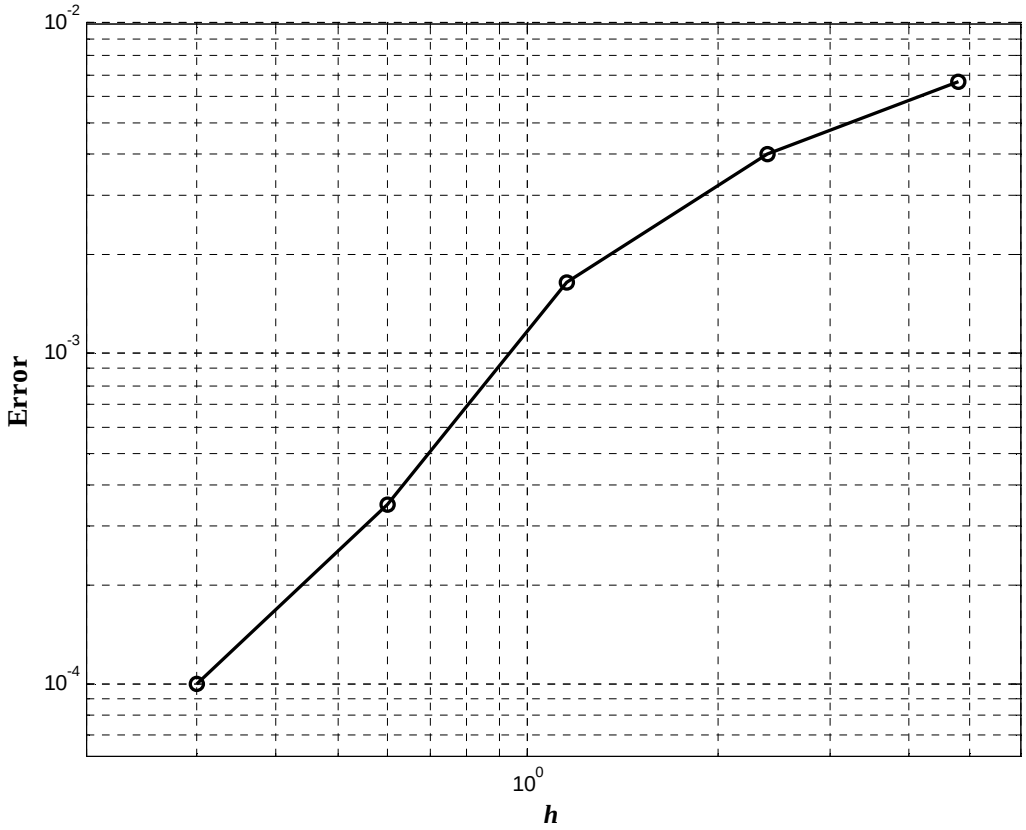

Figure 6 The convergent curve

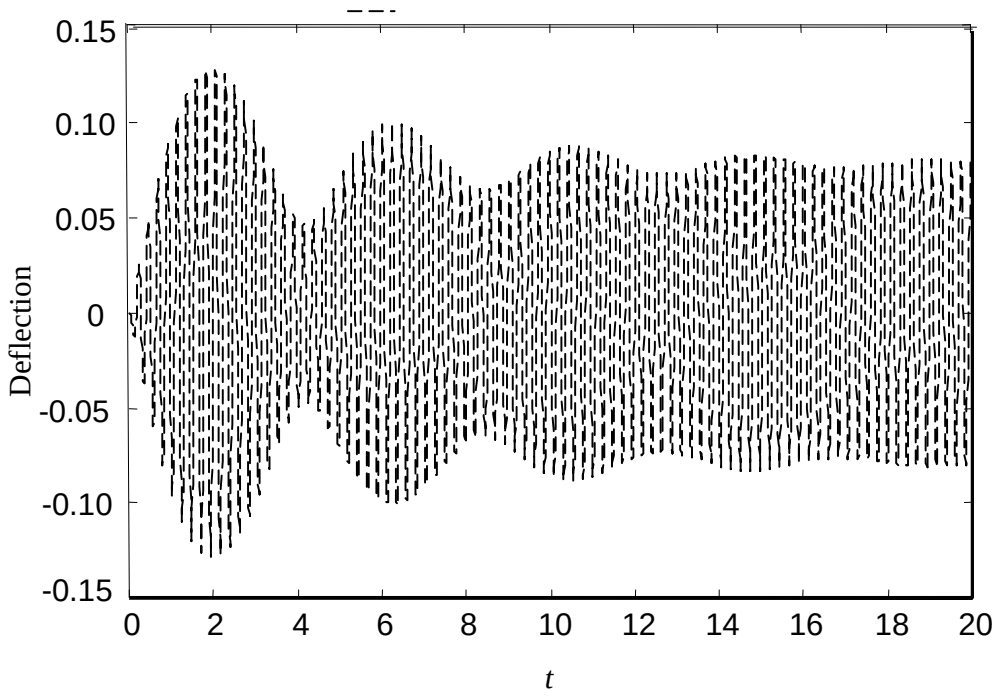

Figure 7 Deflection at free end of the beam obtained by the Newmark method $\Delta t = 5\times10^{-3}$

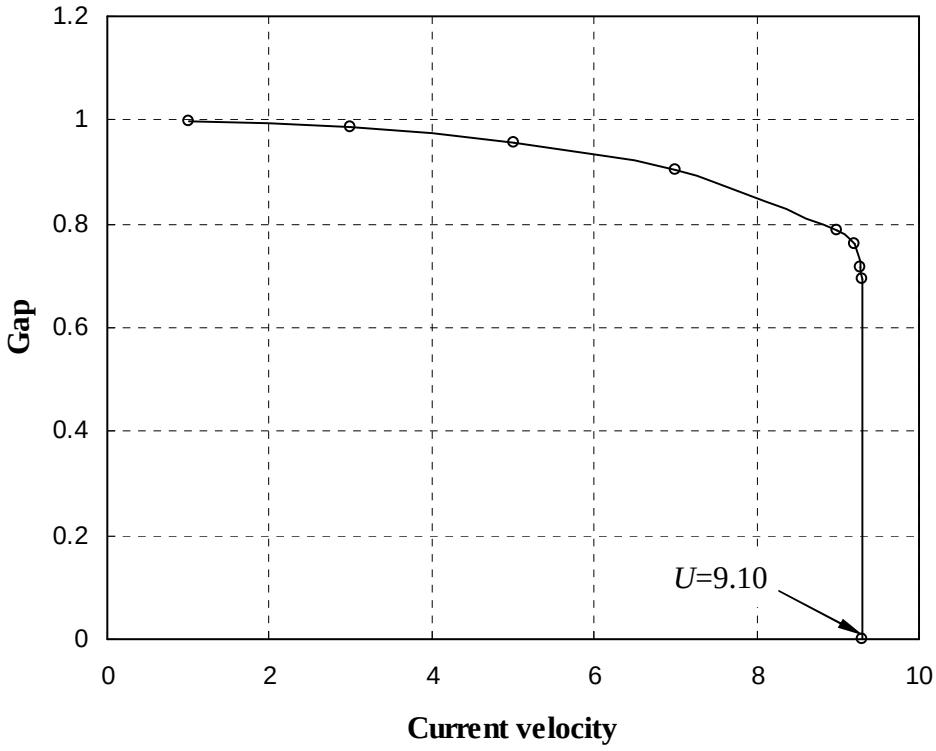

Figure 8 The gap under different current velocities

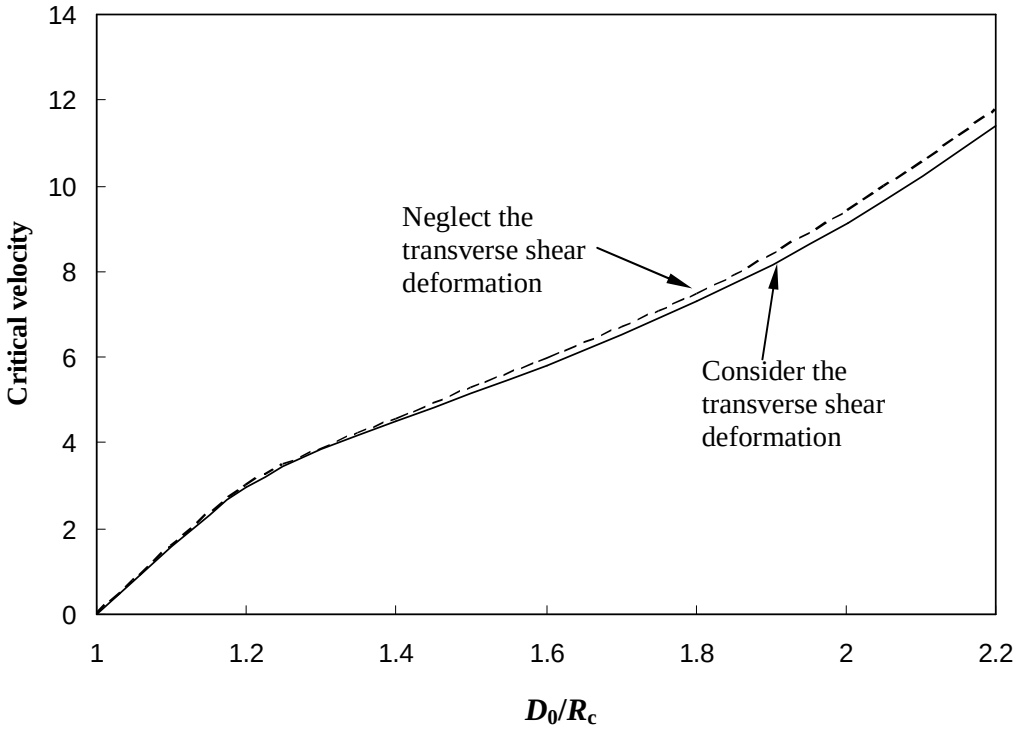

Figure 9 The critical velocities for different initial gaps

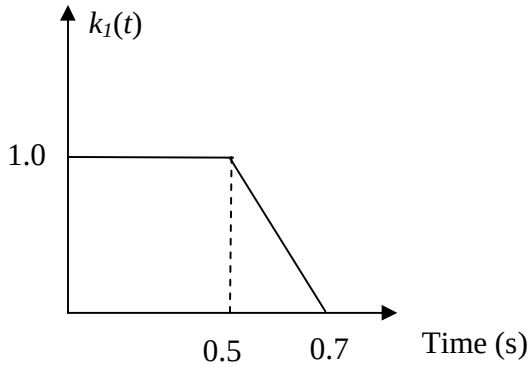

(a) $k_1(t)$

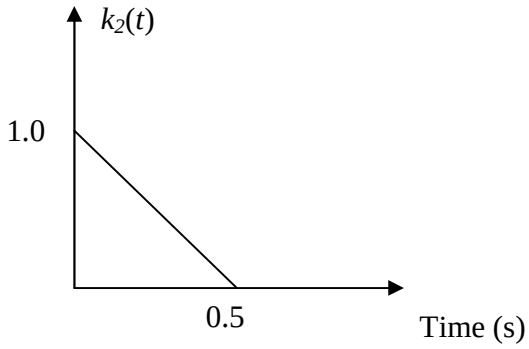

(b) $k_2(t)$

Figure 10 Two cases of the time function $k(t)$

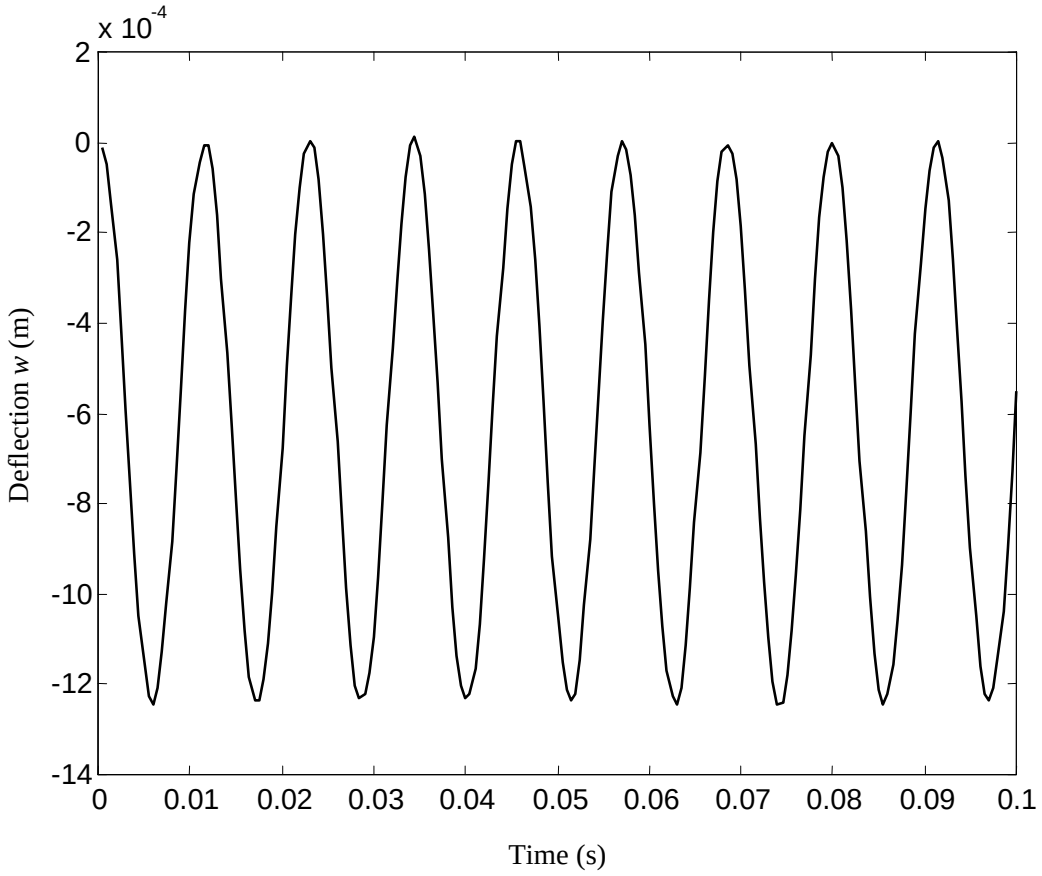

Figure 11 The beginning of dynamic responses of the central point ($x=L/2$) of the pipe ($U(t)=5k_1(t)$)

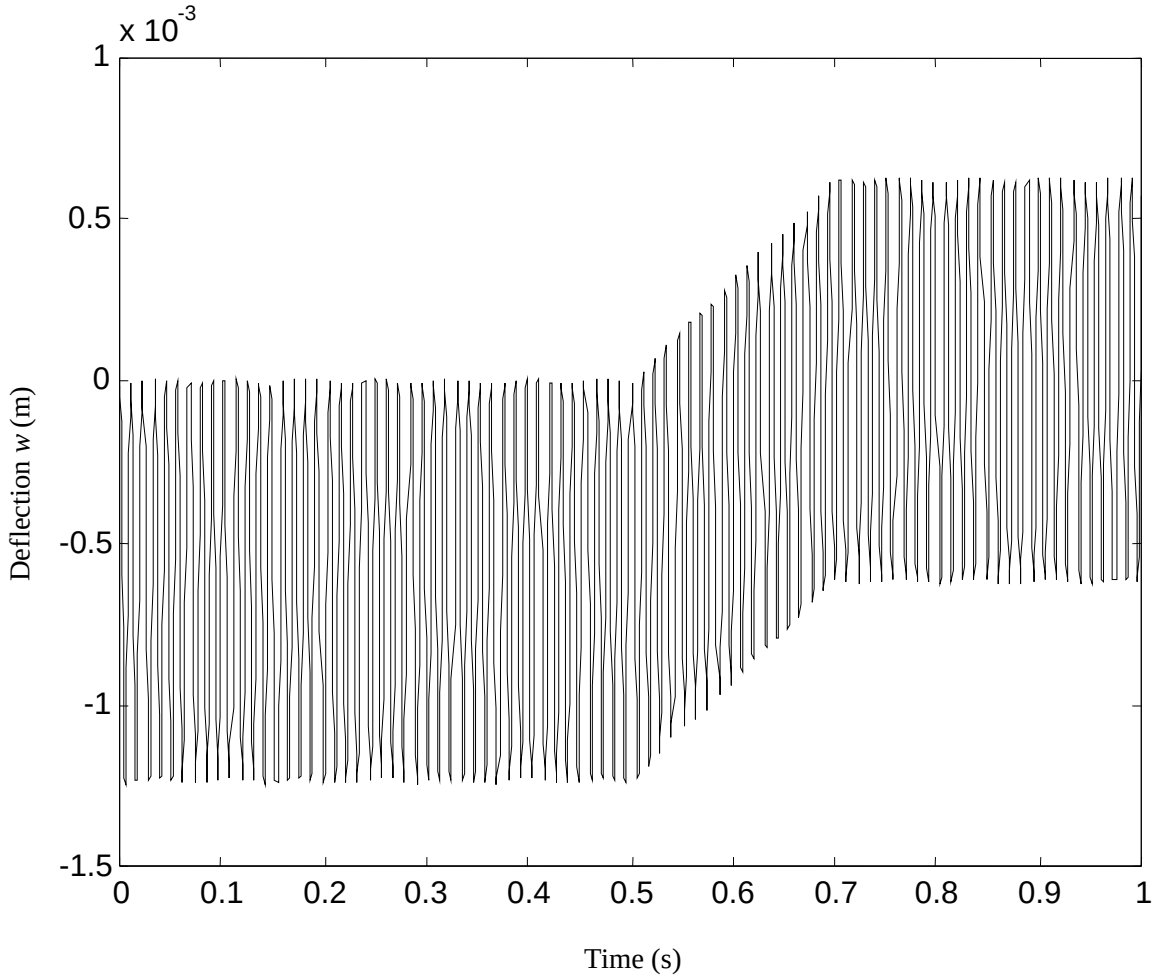

Figure 12 Dynamic responses of the central point ($x=L/2$) of the pipe ($U(t)=5k_1(t)$)

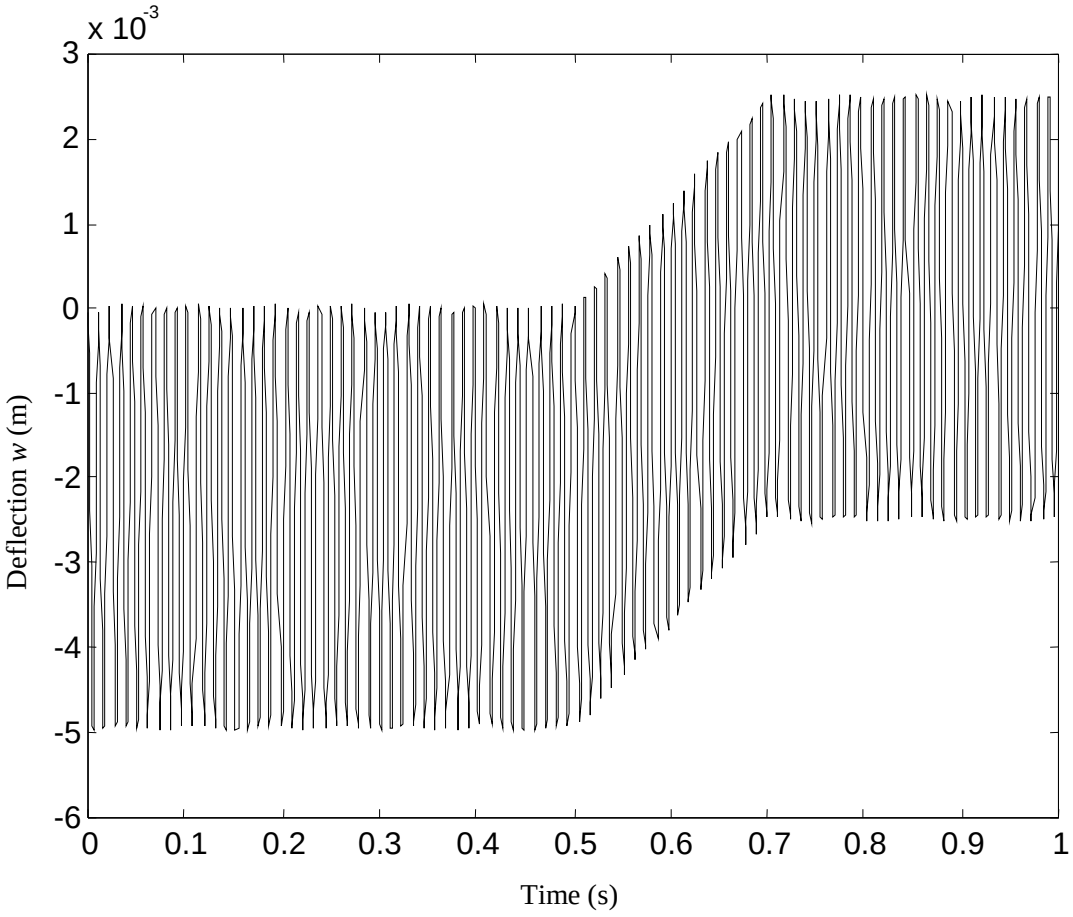

Figure 13 Dynamic responses of the central point (x=L/2) of the pipe ($U(t)$=10$k_1(t)$)

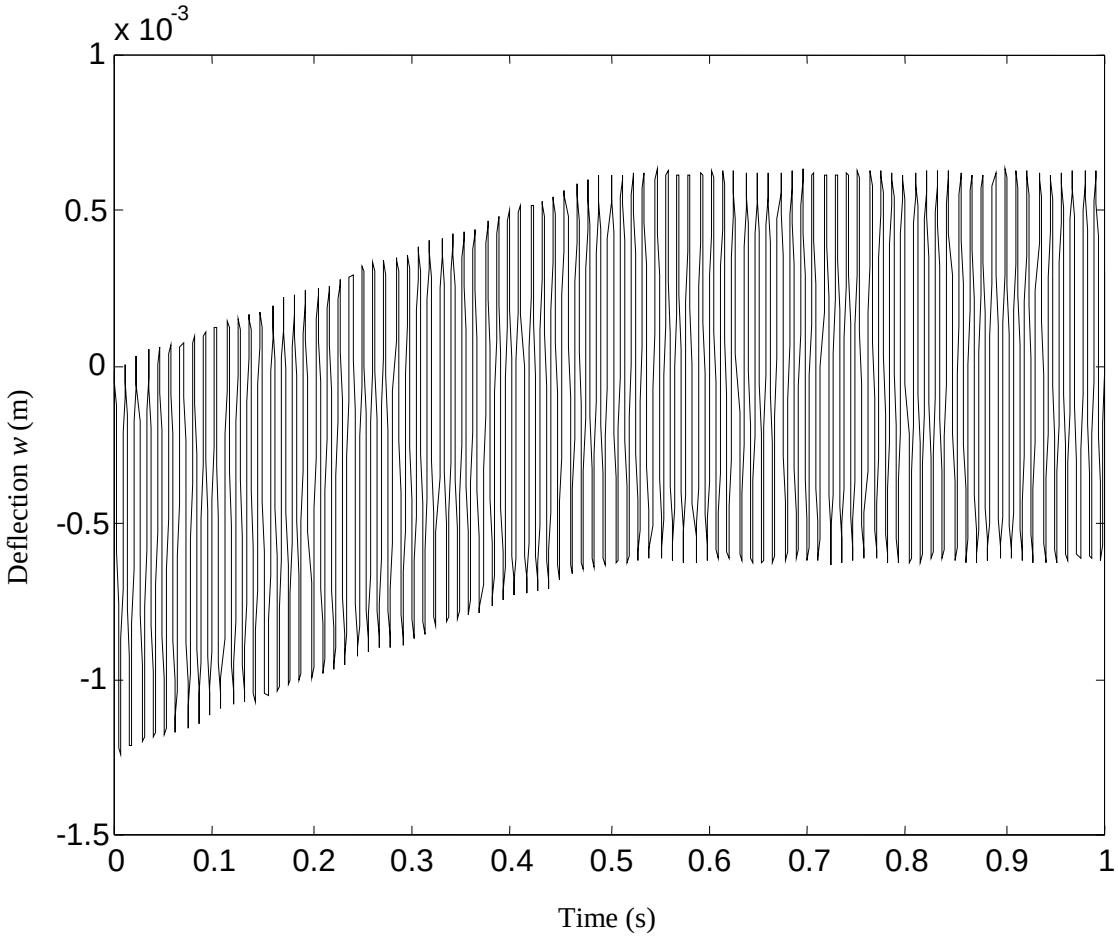

Figure 14 Dynamic responses of the central point ($x=L/2$) of the pipe ($U(t)=5k_2(t)$)

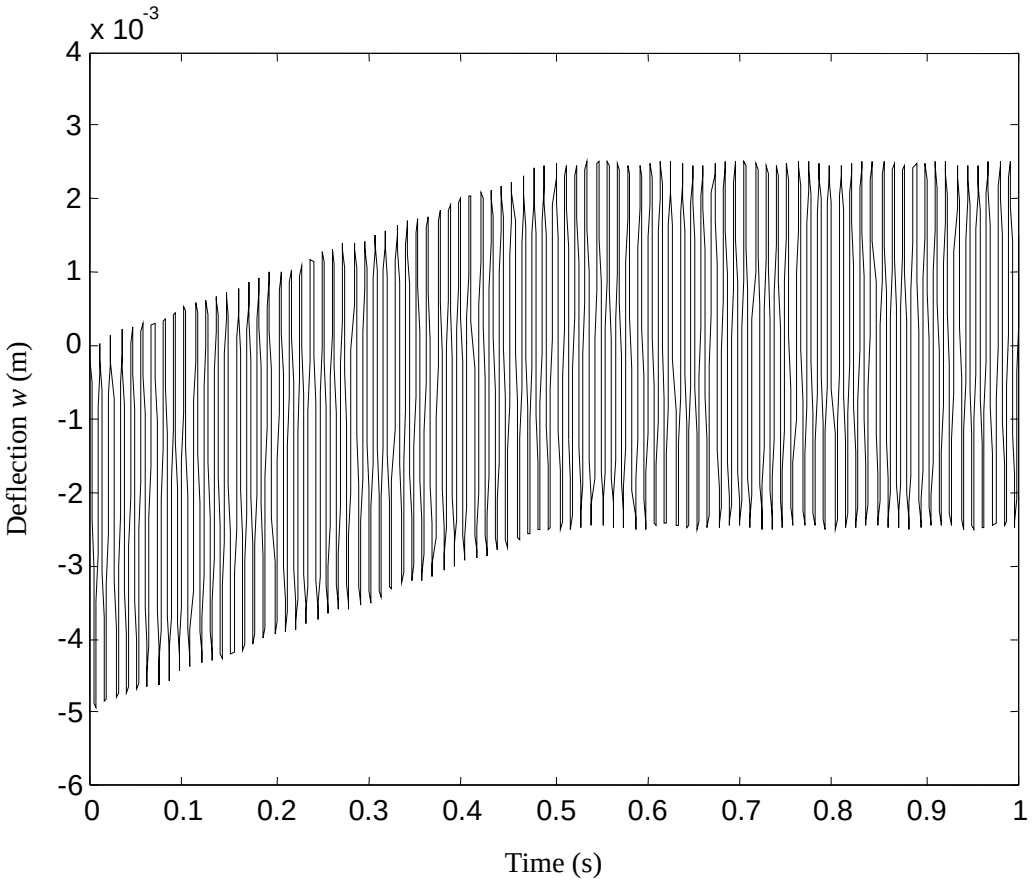

Figure 15 Dynamic responses of the central point ($x=L/2$) of the pipe ($U(t)=10k_2(t)$)

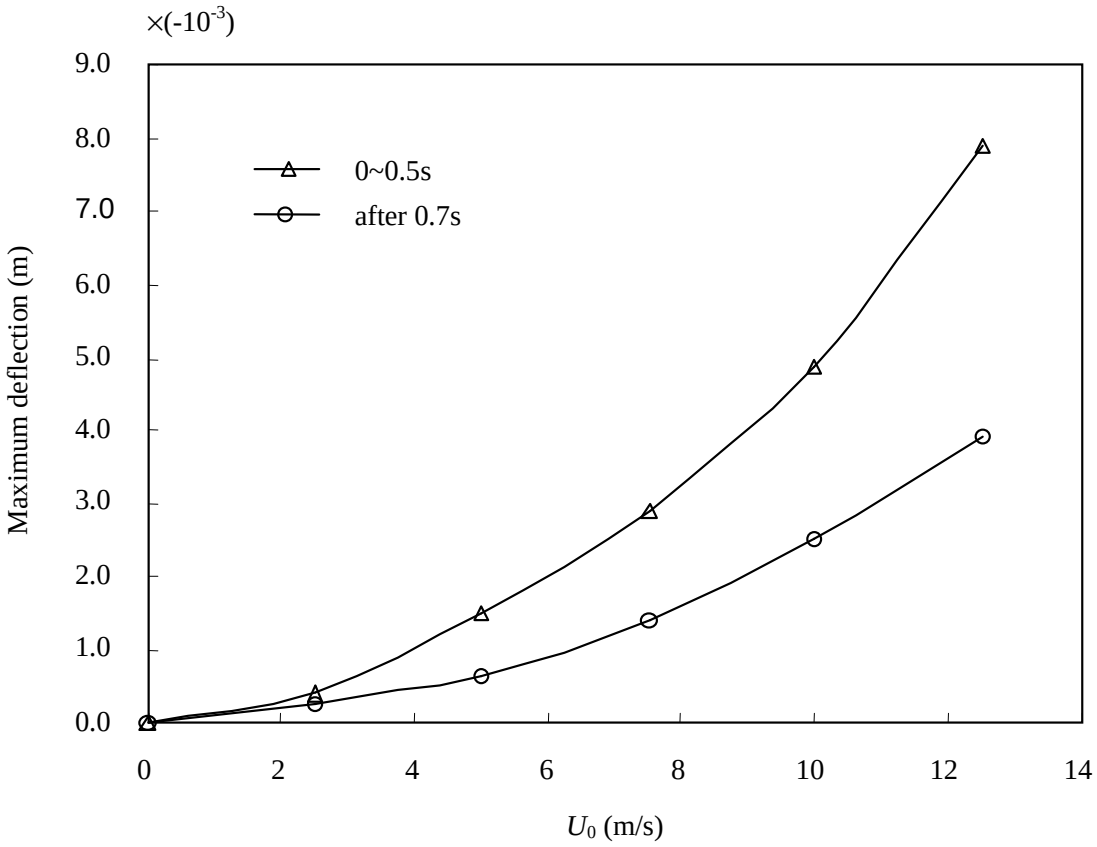

Figure 16 The maximum deflection of the central point ($x=L/2$) of the pipe for different U_0 (for the case of $U(t)=U_0\, k_1(t)$)